



Novel Cr(III) surface magnetic ion-imprinted materials based on graphene oxide for selective removal of Cr(III) in aqueous solution

Huai Li^{a,*}, Jianzheng Li^{b,*}, Long Cheng^{a,c}

^aKey Laboratory of Wetland Ecology and Environment, Northeast Institute of Geography and Agroecology, Chinese Academy of Sciences, Changchun 130012, P.R. China, Tel./Fax: +86 431 85542215; emails: envhit@gmail.com (H. Li),

chenglong13@mailsucas.ac.cn (L. Cheng)

^bState Key Laboratory of Urban Water Resource and Environment, Harbin Institute of Technology, Harbin 150090, P.R. China, Tel./Fax: +86 0451 86283761; email: ljz6677@163.com

^cUniversity of Chinese Academy of Sciences, Beijing 100049, P.R. China

Received 18 August 2014; Accepted 21 February 2015

ABSTRACT

Novel magnetic graphene oxide-based Cr(III) ion-imprinted materials were prepared through surface ionic imprinting technology. The resulting composites were verified by X-ray diffraction, transmission electron microscopy, atomic force microscopy, Fourier transform infrared spectrometer, Raman spectroscopy, and thermogravimetric analysis techniques. Batch adsorption studies were performed to evaluate adsorption kinetics, isotherms, selectivity, and reusability. The intra-particle diffusion model was best described by adsorption kinetics, whereas adsorption equilibrium data were better described by Langmuir equation. Langmuir dimensionless separation factor calculation results indicated highly favorable adsorption with increased adsorption efficiency at higher Cr(III) ion concentrations. The relative selectivity coefficients of Fe₃O₄/SiO₂-GO-IIP for Cr(III)/Na(I), Cr(III)/Mg(II), and Cr(III)/Ca(II) were 2.68, 2.10, and 2.83 times greater than those of Fe₃O₄/SiO₂-GO-NIP, respectively. In addition, reusability without obvious deterioration in performance was demonstrated by the resulting composites in at least five repeated cycles. The experimental results showed that Fe₃O₄/SiO₂-GO-IIP had high affinity and excellent selectivity for Cr(III) ion, as well as reusability and faster magnetic separation under an external magnetic field.

Keywords: Ion imprinting technique; Fe₃O₄/SiO₂-GO; Cr(III) removal; Selectivity; Adsorption

1. Introduction

Heavy metal pollution has become more serious with the rapid increase in global industrial activities. The increase in the presence of heavy metals in the aquatic environment represents a threat to human health, living resources, and ecological systems [1].

One of the major toxic metal ions endangering human life is chromium. Cr(III) compounds are widely used in modern industries, such as leather making, metal finishing, and petroleum refining, which inevitably results in large quantities of Cr(III) ions contaminating industrial effluents. Therefore, a technology for effective Cr(III) removal from water and wastewater is urgently needed.

*Corresponding authors.

Molecular imprinting is a powerful technique for preparing polymeric materials with artificial receptor-like binding sites for various substances [2,3]. Molecular-imprinted polymers (MIPs) have been utilized as materials for molecular recognition in numerous scientific and technical fields, such as solid-phase extraction, chromatography separation, membrane separations, sensors, drug releases, and catalysts [4–7]. Metal ion imprinting technology is a method developed from molecular imprinting, mainly to make selective binding sites in synthetic polymers using a metal ion template. As the template is removed, the remaining polymer becomes more selective [8,9]. Thus, metal ion imprinting technology is an effective and powerful method for the removal of metal ions. Su et al. prepared a Ni(II) ion-imprinted adsorbent to treat heavy metal wastewater based on CS and mycelium [10]. Chen et al. introduced Cr(III) ionic-imprinted polyvinyl alcohol/sodium alginate (PVA/SA) porous composite membranes for selective adsorption of Cr(III) ions [11]. An et al. prepared Cr(III) ionic-imprinting polyamine on silica gel surface for Cr(III) removal [12]. However, these materials cannot be separated rapidly and effectively after wastewater treatment.

Magnetic nanoparticles (MNPs) are ideal candidates for biological and environmental applications because they have unique magnetic properties that enable them to be handled in a magnetic field, and therefore, allow the separation of the target from the samples [13]. Combination of the magnetically susceptible characteristics of MNPs and the unique characteristics of MIPs are expected to provide selectivity for the target molecule and the ability for one-step separation. Jing et al. [14] synthesized magnetic molecularly imprinted nanoparticles for recognition of lysozymes. Kan et al. [15] reported the synthesis of core-shell micro-nanostructured magnetic MIPs for protein recognition. Ren et al. [16] described a magnetic Cu(II) ion-imprinted composite adsorbent for selective removal of copper. Based on previous studies, the present work aims to develop further the route to prepare functional materials.

Graphene oxide (GO) is a strongly oxygenated, highly hydrophilic layered material containing functional groups, such as $-\text{COOH}$, $-\text{C}=\text{O}$, and $-\text{OH}$, on its surface. GO has the potential to act as an inorganic support material in synthesizing surface-imprinting polymer due to its unique intensity, special structure, and stable chemical properties. Magnetic graphene oxide-based composites that take advantage of the superior properties of graphene and certain functional materials provide a new way to develop ion-imprinted materials. However, they have not been extensively

explored to date. In this study, we report firstly ion-imprinted polymer (IIP)-functionalized magnetic graphene oxide hybrid material ($\text{Fe}_3\text{O}_4/\text{SiO}_2\text{-GO-IIP}$) by surface molecular printing technique, as well as its sensing property. $\text{Fe}_3\text{O}_4/\text{SiO}_2\text{-GO}$ was used to synthesize novel $\text{Fe}_3\text{O}_4/\text{SiO}_2\text{-GO-IIP}$ by metal ion imprinting technology, characterized through AEM, TEM, XRD, TGA, FTIR, and Raman spectroscopy. Investigations for the removal of Cr(III) ions through adsorption kinetics, isotherms, selective adsorption in multi-ion solution, and reuse were carried out to understand the mechanism of Cr(III) ion adsorption onto $\text{Fe}_3\text{O}_4/\text{SiO}_2\text{-GO-IIP}$.

2. Material and methods

2.1. Materials and instruments

Chemical-grade polyethyleneimine (PEI, $M_w = 7 \times 10^4$) was purchased from Qianglong Chemical Limited Company, Wuhan, China. Epichlorohydrin (ECH) was received from Beijing Chemical Plant. All other necessary chemicals were of analytical grade and purchased from the Chemical Reagent Company of Harbin. All dilutions were made with distilled water.

The samples were characterized by TEM (JEOL 2011, 200 kV), AFM (Digital Instrument Nanoscope IIIa, in tapping mode), Raman spectrometry (Jobin Yvon HR 800, with laser excitation at 457.9 nm), and FTIR (Avatar 360, with a resolution of 2 cm^{-1}). The method for preparing species before AFM test is that the $\text{Fe}_3\text{O}_4/\text{SiO}_2\text{-GO}$ and $\text{Fe}_3\text{O}_4/\text{SiO}_2\text{-GO-IIP}$ nanoparticles were dispersed on mica until dry in the air using alcohol as solvent. TGA was performed by heating the samples in nitrogen or air flow at a rate of 100 mL/min using a Perkin-Elmer Diamond TG/DTA thermal analyzer with a heating rate of $10^\circ\text{C}/\text{min}$. XRD patterns of all samples were obtained on a Bruker D8-Advance X-ray diffractometer with Cu K α radiation ($k = 1.5418 \text{ \AA}$) at an accelerating voltage and current of 40 kV and 40 mA, respectively. The concentration of chromium ions was analyzed using Perkin-Elmer 3110 atomic absorption spectrometry, a Thermo Scientific ICP 6000 Series ICP system.

2.2. Preparation of ion-imprinted materials

The preparation process for the ion-imprinted materials was as follows. First, $\text{Fe}_3\text{O}_4/\text{SiO}_2\text{-GO}$ nanocomposites were prepared using a previously reported method [17]. $\text{Fe}_3\text{O}_4/\text{SiO}_2\text{-GO-PEI}$ were prepared according to reported procedure [18], but with some modifications. The typical preparation process was as follows: $\text{Fe}_3\text{O}_4/\text{SiO}_2\text{-GO}$ nanoparticles were

dispersed in deionized water (50 mL) by ultrasonication, and then cationic reagent PEI (1% PEI aqueous solution) was added to the solution, and then vigorous stirring for 12 h. Afterward, excess PEI was washed out. Then, 200 mg Fe₃O₄/SiO₂-GO-PEI was mixed with a certain amount of Cr(III) solution with a concentration of 100 mg/L. The pH of the medium was adjusted to 6 using NaAc–HAc buffer solution, and the mixture was shaken in a constant-temperature shaker for a certain period of time until the PEI grafted on Fe₃O₄/SiO₂-GO was fully swollen and the chelation adsorption reached equilibrium. After filtration, Fe₃O₄/SiO₂-GO-PEI particles that adsorbed the saturated Cr(III) was washed repeatedly with water until Cr(III) could not be detected in the filtrate, after which they were dried in a vacuum oven. Then, 200 mg Fe₃O₄/SiO₂-GO-PEI-adsorbed Cr(III) and 10 mL of ECH were added into absolute ethanol. The reaction was allowed to continue for 30 min at room temperature (25°C) with continuous stirring. Afterward, 10 mL of sodium hydroxide (0.01 M) was added. The reaction continued for 90 min at room temperature with continuous stirring. Finally, particles were fully washed with 0.1 M hydrochloric acid solution to remove the template ion, and the novel Cr(III) ion-imprinted materials were obtained. To put it briefly, a route of synthesis for the ion-imprinted materials was as follows. Firstly Fe₃O₄/SiO₂-GO nanocomposites were prepared, secondly Fe₃O₄/SiO₂-GO-PEI were synthesized, thirdly Fe₃O₄/SiO₂-GO-PEI particles adsorbed Cr(III) and ECH were added to crosslinking, and then, the template ion was washed. The non-imprinted materials (Fe₃O₄/SiO₂-GO-NIP) were prepared similarly, except for the Cr(III) imprinting and removal process.

2.3. Adsorption studies

To investigate the adsorption dynamics of Fe₃O₄/SiO₂-GO-IIP (i.e. Fe₃O₄/SiO₂-GO-NIP), 10 mg imprinted polymer was dispersed in 10 mL aqueous solution of Cr(III) with concentration (C_0) of 1 mg/L. The mixture was shaken continuously at 25°C. The specimens were sampled at different time intervals as follows: 5, 10, 15, 25, 35, and 50 min. The adsorption efficiency and capacity were calculated based on the difference of Cr(III) concentrations before and after adsorption. To investigate the adsorption equilibrium of Fe₃O₄/SiO₂-GO-IIP (i.e. Fe₃O₄/SiO₂-GO-NIP), 4 mg imprinted polymer was equilibrated with varied initial concentrations (0.25, 0.5, 1, 2, and 4 mg/L) of Cr(III) in each tube. After 1 h, the saturated polymer was separated by a strong magnet. The clear solutions were then collected and subjected to ICP analysis to determine the final chromium concentrations.

Adsorption values were calculated from the change in solution concentration using the following equation [19]:

$$q = \frac{(C_0 - C_e)V}{W} \quad (1)$$

where q (mg/g) is the adsorption capacity; C_0 (mg/L) and C_e (mg/L) are the initial and equilibrated metal ion concentrations, respectively, V (L) is the volume of added solution; and W (g) is the mass of the adsorbent (dry).

$$E = \frac{C_0 - C_e}{C_0} \times 100\% \quad (2)$$

where E (%) is the removal efficiency.

To estimate the selectivity of Fe₃O₄/SiO₂-GO-IIP for Cr(III), 4 mg Fe₃O₄/SiO₂-GO-IIP and Fe₃O₄/SiO₂-GO-NIP were dispersed in 4 mL aqueous solutions containing 1 mg/L Cr(III), Na(I), Mg(II), and Ca(II) respectively. The mixture was shaken at 25°C for 1 h. After adsorption equilibrium, the concentrations of Cr(III), Na(I), Mg(II), and Ca(II) were determined by ICP analysis. Distribution and selectivity coefficients of Na(I), Mg(II), and Ca(II) with respect to Cr(III) were calculated according to the following equation [20]:

$$K_d = \left(\frac{C_0 - C_e}{C_e} \right) \frac{V}{W} \quad (3)$$

where K_d is the distribution coefficient (L/g).

$$K = \frac{K_d(\text{Cr(III)})}{K_d(M)} \quad (4)$$

where K is the selectivity coefficient and M represents Na(I), Mg(II), or Ca(II) ions. A comparison of the K values of Fe₃O₄/SiO₂-GO-IIP with these metal ions allows an estimation of the imprinting effect on selectivity. A relative selectivity coefficient (K') is an indicator that expresses metal adsorption affinity of recognition sites to the imprinted Cr(III) ions, which can be defined by Eq. (5) as follows:

$$K' = \frac{K_{\text{imprinted}}}{K_{\text{non-imprinted}}} \quad (5)$$

where $K_{\text{imprinted}}$ and $K_{\text{non-imprinted}}$ are the selectivity coefficients of Fe₃O₄/SiO₂-GO-IIP and Fe₃O₄/SiO₂-GO-NIP, respectively.

2.4. Desorption and reuse

Desorption of Cr(III) ions from Fe₃O₄/SiO₂-GO-IIP was studied using 0.1 M HCl as a desorbing agent after exhaustion by sole Cr(III), Cr(III)/Na(I), Cr(III)/Na(I)/Mg(II), Cr(III)/Na(I)/Ca(II), and Cr(III)/Na(I)/Mg(II)/Ca(II) mixed solution with each metal concentration of 1 mg/L, respectively. The 4 mg metal-loaded Fe₃O₄/SiO₂-GO-IIP samples were placed in 4 mL of 0.1 M HCl shaken for 1 h at 25°C. The Cr(III) ion concentrations in the solution were analyzed at desorption equilibrium.

After each adsorption–desorption cycle, Fe₃O₄/SiO₂-GO-IIP was regenerated using 0.1 M HCl aqueous solutions numerous times until traces of Cr(III) could not be detected in the filtrate. Subsequently, the adsorbents were washed thoroughly with distilled water to achieve neutrality, and then dried in a vacuum oven at 50°C for adsorption in the succeeding cycle.

3. Results and discussion

3.1. Characterization of Cr(III) ion-imprinted materials

The XRD patterns of GO, magnetite, Fe₃O₄/SiO₂-GO, and Fe₃O₄/SiO₂-GO-IIP, which displayed several relatively strong reflection peaks in the 2θ region of 5°–80° were compared in Fig. 1. The as-prepared Fe₃O₄/SiO₂-GO hybrid composite presented diffraction peaks of Fe₃O₄ when combined with GO. The

peak positions were unchanged upon coating of polymerization, indicating that the crystalline structures of the magnetite and GO were essentially maintained.

Raman spectroscopy is a useful tool for identifying carbon materials. Fig. 2 shows the Raman spectra of Fe₃O₄/SiO₂-GO, Fe₃O₄/SiO₂-GO-PEI, and Fe₃O₄/SiO₂-GO-IIP. In the three samples, two prominent peaks were clearly visible, namely G peak and D peak, which corresponded to the Brillouin zone-centered LO-phonon around 1,575 cm⁻¹ and to the double-resonance excitation of phonons close to the K point in the Brillouin zone around 1,360 cm⁻¹ [21], respectively. The intensity ratio (*I*_D/*I*_G) was characterized by the extent of disorder present within the material [22,23]. For our samples, the *I*_D/*I*_G ratios of Fe₃O₄/SiO₂-GO, Fe₃O₄/SiO₂-GO-PEI, and Fe₃O₄/SiO₂-GO-IIP were 0.673, 0.757, and 0.980, respectively, which reflected the increase in disorder. Compared with the G-bands of Fe₃O₄/SiO₂-GO and Fe₃O₄/SiO₂-GO-IIP, the G-band of Fe₃O₄/SiO₂-GO-IIP clearly occurred at 1,571 cm⁻¹, which was downshifted by 5 cm⁻¹ compared with that of Fe₃O₄/SiO₂-GO. The Raman shifts of the G band for Fe₃O₄/SiO₂-GO-IIP provided evidence for the charge transfer of Fe₃O₄/SiO₂-GO and IIP, which suggested a strong interaction between the two.

The FTIR spectra of Fe₃O₄/SiO₂-GO, Fe₃O₄/SiO₂-GO-PEI, and Fe₃O₄/SiO₂-GO-IIP were measured and shown in Fig. 3. The characteristic of Si–O–Si peak (1,091 cm⁻¹, 468 cm⁻¹), Fe–O (576 cm⁻¹), and aromatic C=C (1,621 cm⁻¹) was the direct evidence needed to

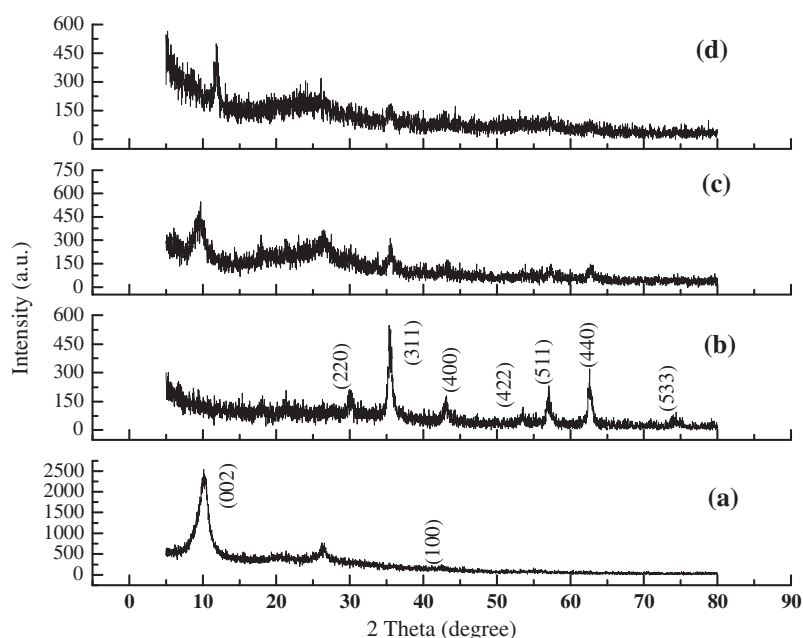


Fig. 1. XRD patterns of (a) GO, (b) Fe₃O₄, (c) Fe₃O₄/SiO₂-GO, and (d) Fe₃O₄/SiO₂-GO-IIP.

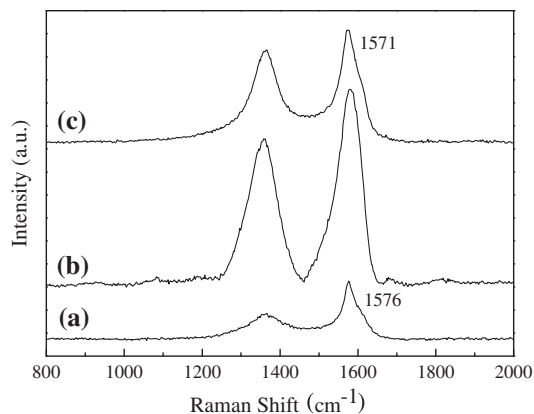


Fig. 2. Raman spectra of (a) Fe₃O₄/SiO₂-GO, (b) Fe₃O₄/SiO₂-GO-PEI, and (c) Fe₃O₄/SiO₂-GO-IIP.

consolidate the formation of Fe₃O₄/SiO₂-GO. Absorption peaks at 1,300 and 774 cm⁻¹, which were vibration absorptions of the N–H bond, and at 1,467 and 1,570 cm⁻¹ (C–N stretch of amide) appeared, indicating that PEI was bound to the surfaces of Fe₃O₄/SiO₂-GO. The absorption peak at 1,066 cm⁻¹ was strengthened distinctly after ion imprinting, which was the characteristic absorption of the C–N bond of tertiary amine groups. By contrast, the absorption peak at 1,300 and 774 cm⁻¹, which were vibration absorptions of N–H bond, disappeared. The disappearance of these peaks revealed that the H atoms of the primary and secondary amine groups in PEI chains had been substituted completely by methylene of ECH (via ring opening reaction and dehydrochlorination reaction). This finding suggests that all of the

primary and secondary amine groups in the PEI chains had changed into tertiary groups. Simultaneously, the vibration absorption of C–OH bond groups appeared at 1,504, 1,375, and 695 cm⁻¹, indicating further that the ring-opening reaction of ECH had occurred. These findings showed that the crosslinking between macromolecules of PEI were produced by the effect of the cross-linker ECH. In addition, a layer of IIP that formed on the surfaces of Fe₃O₄/SiO₂-GO was obtained.

The TGA curves of Fe₃O₄/SiO₂-GO and Fe₃O₄/SiO₂-GO-IIP are given in Fig. 4. Fe₃O₄/SiO₂-GO was thermally stable, and the mass loss started above 150°C. Weight loss again increased rapidly beyond 200°C during the removal of the functional groups (–OH and –COOH) from Fe₃O₄/SiO₂-GO [24]. For Fe₃O₄/SiO₂-GO-IIP, the rate of weight loss increased below 100°C owing to the thermal decomposition of the ECH. The high rate of weight loss in temperatures ranging from 100 to 200°C may be due to the dehydration in the layer of Fe₃O₄/SiO₂-GO-IIP. Fe₃O₄/SiO₂-GO-IIP exhibited a rapid weight loss rate of 299°C, which originated from the imprinted polymer on the surface of Fe₃O₄/SiO₂-GO. Moreover, the weight loss of Fe₃O₄/SiO₂-GO-IIP obtained from the TGA analysis was 71.27 wt.%, which was much more than that of Fe₃O₄/SiO₂-GO (26.86 wt.%). The results fully demonstrated the existence of imprinted polymer.

The morphological structures of Fe₃O₄/SiO₂-GO and Fe₃O₄/SiO₂-GO-IIP were examined by TEM. Based on the TEM image (Fig. 5(a)), Fe₃O₄/SiO₂-GO resembled wrinkled paper, was very thin, and contained numerous wrinkles. These wrinkles may be

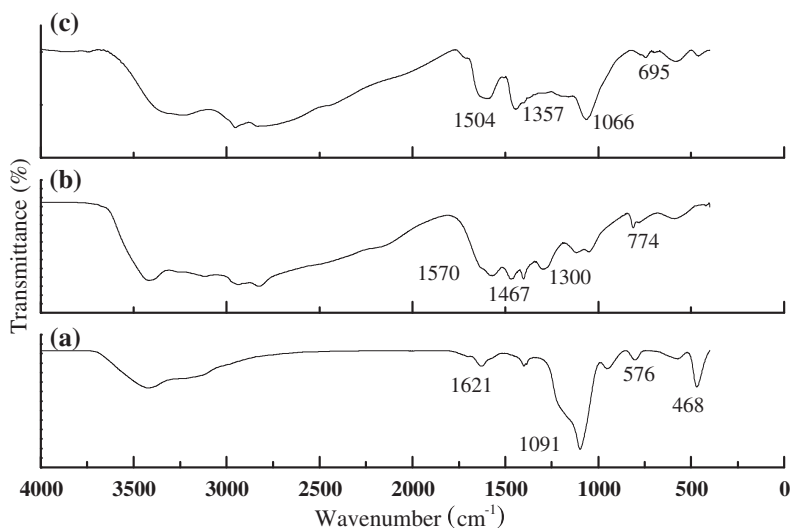


Fig. 3. FT-IR spectra of (a) Fe₃O₄/SiO₂-GO, (b) Fe₃O₄/SiO₂-GO-PEI, and (c) Fe₃O₄/SiO₂-GO-IIP.

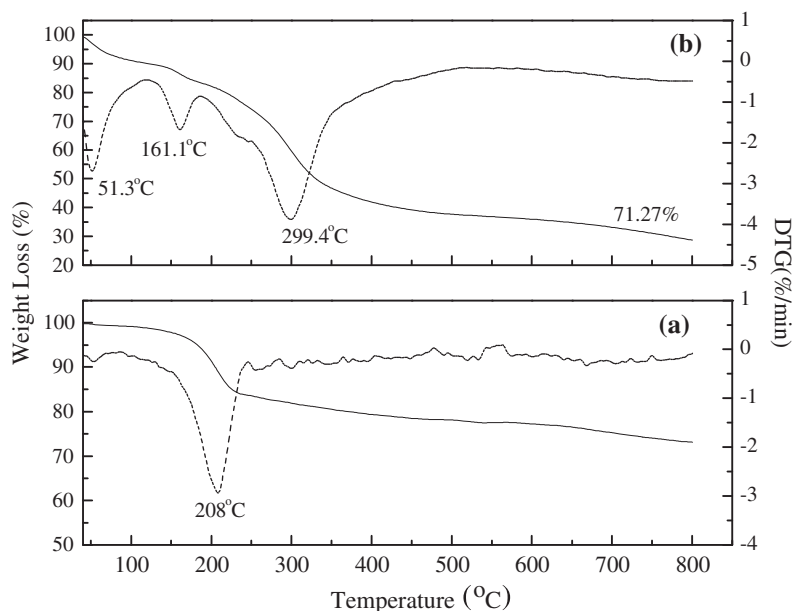


Fig. 4. TG and DTG curves of (a) Fe₃O₄/SiO₂-GO and (b) Fe₃O₄/SiO₂-GO-IIP with a heating rate of 10°C/min in nitrogen atmosphere.

important for preventing aggregation of GO and in maintaining a high surface area [25]. As seen in Fig. 5(b), Fe₃O₄/SiO₂-GO was almost covered by the IIP films, which indicated that the imprinted sites were generated in the Fe₃O₄/SiO₂-GO-IIP hybrid. The surfaces of the IIP films were probed using AFM. The height of Fe₃O₄/SiO₂-GO as measured from the cross-section analysis was 2 nm or so (Fig. 5(c)). According to AFM imaging of Fe₃O₄/SiO₂-GO-IIP (Fig. 5(d)), the average thickness of the polymer grafted on the Fe₃O₄/SiO₂-GO surface was about 3 nm. Fig. 6 shows the efficient magnetic separation process within seconds, which was very favorable for the magnetic separation of target pollutants from liquid environments in the aspect of practical engineering.

3.2. Adsorption kinetics and isotherms

An equilibrium binding analysis was carried out to investigate the binding performance of Fe₃O₄/SiO₂-GO-IIP. Fig. 7 shows the dynamic binding curves of Fe₃O₄/SiO₂-GO-IIP and Fe₃O₄/SiO₂-GO-NIP. Fe₃O₄/SiO₂-GO-IIP clearly reached its binding equilibriums at about 25 min, indicating a fast binding process. Compared with Fe₃O₄/SiO₂-GO-NIP, a much higher adsorption capacity was achieved on Fe₃O₄/SiO₂-GO-IIP. The curve of Fe₃O₄/SiO₂-GO-IIP indicated that molecular imprinting resulted in the formation of specific recognition sites on the surface of Fe₃O₄/SiO₂-GO-IIP, which benefited Cr(III) in binding with the

recognition sites and imparted small mass-transfer resistance.

The prediction of adsorption rate provides important information for selecting optimum operating conditions for full-scale batch process. To investigate the mechanism of adsorption kinetics, pseudo-first-order [26], pseudo-second-order [27], Elovich [28], and intraparticle diffusion [29] kinetic models were tested to interpret data obtained from batch experiments. Their linear forms are as follows:

$$\log(Q_e - Q_t) = \log Q_e - \frac{k_1}{2.303} t \quad (6)$$

$$\frac{t}{Q_t} = \frac{1}{k_{ad} Q_e^2} + \frac{t}{Q_e} \quad (7)$$

$$Q_t = \frac{1}{\beta} \ln(\alpha\beta) + \frac{1}{\beta} \ln(t) \quad (8)$$

$$Q_t = k_{dif} t^{0.5} + C \quad (9)$$

where Q_t is the solid-phase loading of Cr(III) in the adsorbent at time t , Q_e is the adsorption capacity at equilibrium, k_1 is the rate constant of pseudo-first-order adsorption, and k_{ad} is the pseudo-second-order adsorption rate constant. α and β represent the initial adsorption rate and desorption constant in the Elovich model, k_{dif} indicates the intraparticle diffusion rate

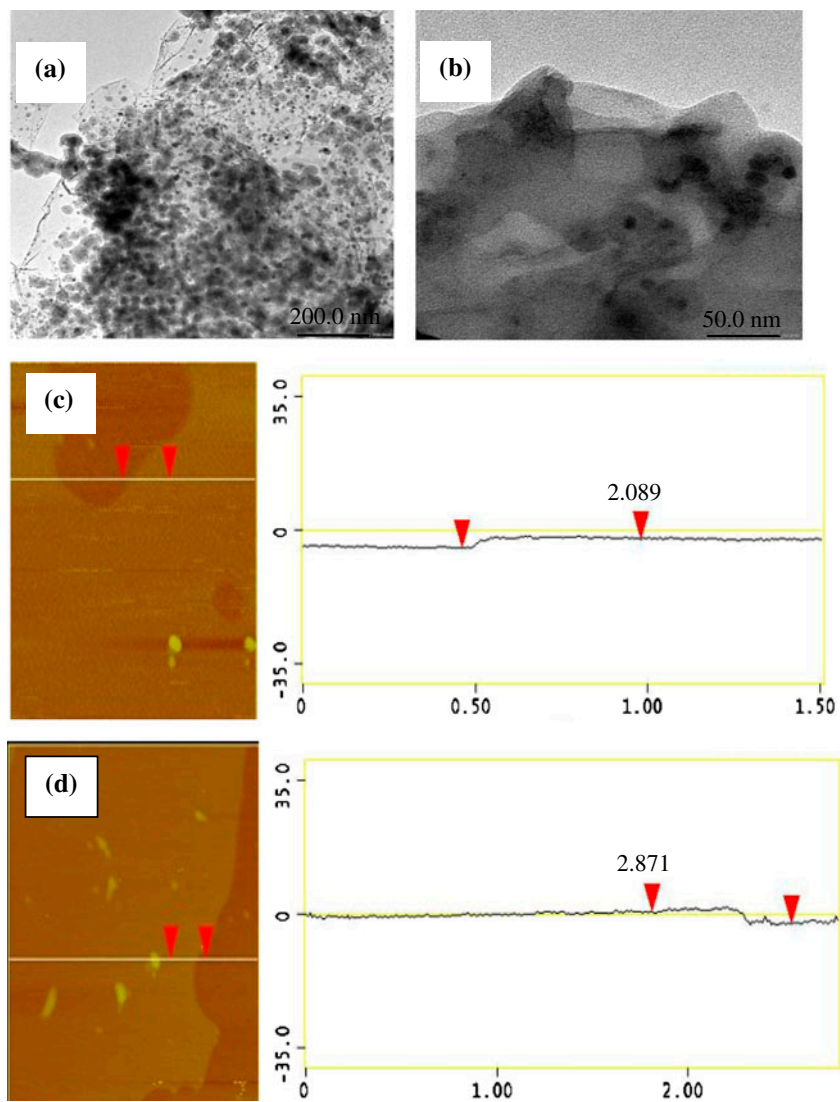


Fig. 5. TEM images of (a) $\text{Fe}_3\text{O}_4/\text{SiO}_2\text{-GO}$ and (b) $\text{Fe}_3\text{O}_4/\text{SiO}_2\text{-GO-IIP}$. Tapping-mode AFM images of (c) $\text{Fe}_3\text{O}_4/\text{SiO}_2\text{-GO}$ and (d) $\text{Fe}_3\text{O}_4/\text{SiO}_2\text{-GO-IIP}$ dispersion dip-coated on mica.

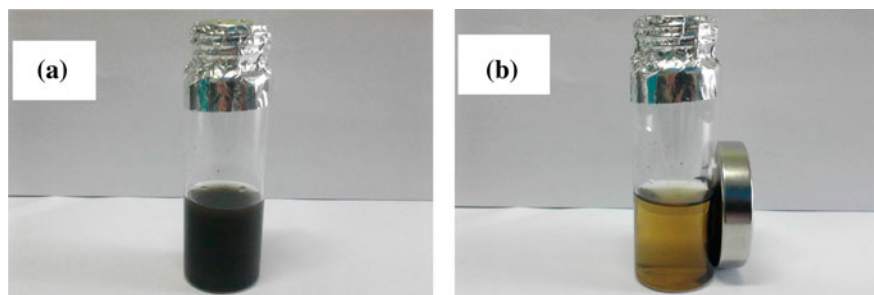


Fig. 6. Photographs of the separation and dispersion processes of $\text{Fe}_3\text{O}_4/\text{SiO}_2\text{-GO-IIP}$: (a) without external magnetic field and (b) with external magnetic field.

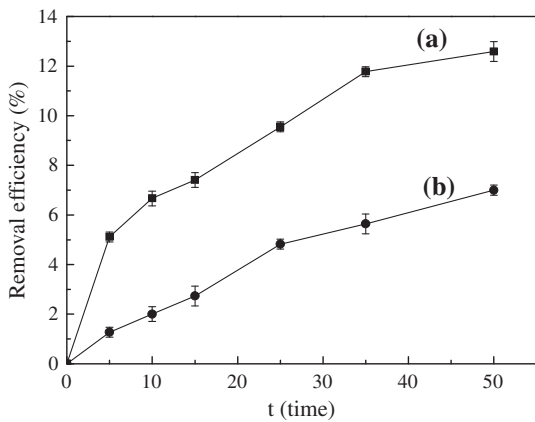


Fig. 7. Adsorption kinetic curves of (a) Fe₃O₄/SiO₂-GO-IIP and (b) Fe₃O₄/SiO₂-GO-NIP for Cr(III).

constant, and C provides information about the thickness of the boundary layer.

As seen in Fig. 8, the correlation coefficients (R^2) given by the four kinetic models were 0.951, 0.9673, 0.9516, and 0.9918, respectively. The intraparticle diffusion kinetic model provided good correlation for the adsorption of Cr(III) ions on Fe₃O₄/SiO₂-GO-IIP. Moreover, the plots did not go through the origin, which indicated that the adsorption mechanism of

Cr(III) ions on Fe₃O₄/SiO₂-GO-IIP was a multistep, limited adsorption process. The adsorption kinetic constants and linear regression equations are summarized in Table 1.

Adsorption isotherm can be utilized to obtain information about the interaction between adsorbent and adsorbate molecules; it can also be used to predict the relative performance of different types of adsorbents. To understand and clarify the adsorption process, Langmuir adsorption isotherm and Freundlich adsorption isotherm models were used in this study.

The Langmuir and Freundlich isotherms are represented by

$$\frac{1}{q_e} = \frac{1}{q_{\max}} + \frac{1}{q_{\max}K_1C_e} \quad (10)$$

$$\log q_e = \log K_F + \frac{1}{n} \log C_e \quad (11)$$

where q_{\max} and K_1 are the Langmuir parameters. q_{\max} represents the maximum adsorption capacity and K_1 is the Langmuir constant that represents the affinity between the solute and the adsorbent. n and K_F are the Freundlich parameters for values that range from $1 < n < 10$, indicating that adsorption is favorable.

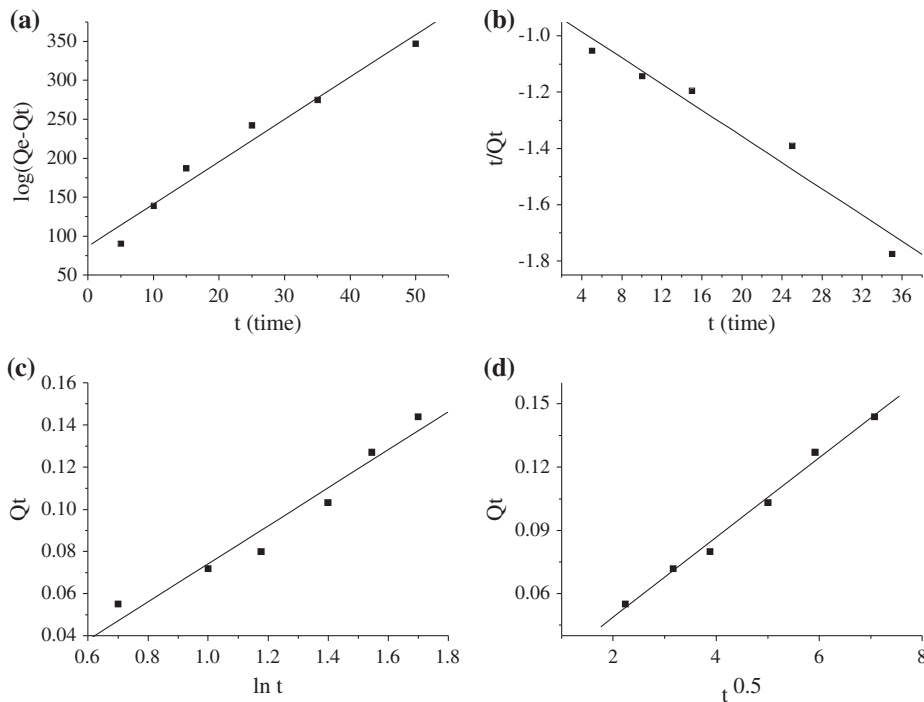


Fig. 8. The linear plot of (a) $\log(Q_e - Q_t)$ vs. t , (b) t/Q_t vs. t , (c) Q_t vs. $\ln t$, and (d) Q_t vs. $t^{0.5}$.

Table 1
Parameters obtained from different kinetic models

Models	Parameters		R^2
Pseudo-first order	k_1 (min^{-1})	Q_e (mg/g)	0.9510
	0.054	0.13	
Pseudo-second order	k_{ad} (g/mg/min)	Q_e (mg/g)	0.9673
	0.34	0.18	
Elovich	α (mg/g/min)	β (g/mg)	0.9516
	13.2	11.1	
Intraparticle diffusion	k_{dif} (mg/g/min ^{0.5})	C (mg/g)	0.9918
	0.019	0.011	

The results of the adsorption isotherms are listed in Fig. 9 and Table 2. As illustrated in Fig. 9, the equilibrium adsorption capacity of $\text{Fe}_3\text{O}_4/\text{SiO}_2\text{-GO-IIP}$ and $\text{Fe}_3\text{O}_4/\text{SiO}_2\text{-GO-NIP}$ increased rapidly and reached complete equilibrium by increasing the original concentration. The adsorption capacity of $\text{Fe}_3\text{O}_4/\text{SiO}_2\text{-GO-IIP}$ was about three times higher than that of $\text{Fe}_3\text{O}_4/\text{SiO}_2\text{-GO-NIP}$. The adsorption data could be described well by the Langmuir model ($R^2 = 0.9929$) rather than the Freundlich model ($R^2 = 0.9891$), which implied homogenous distribution of imprinting sites on the $\text{Fe}_3\text{O}_4/\text{SiO}_2\text{-GO-IIP}$ surface (Fig. 10). q_{max} value,

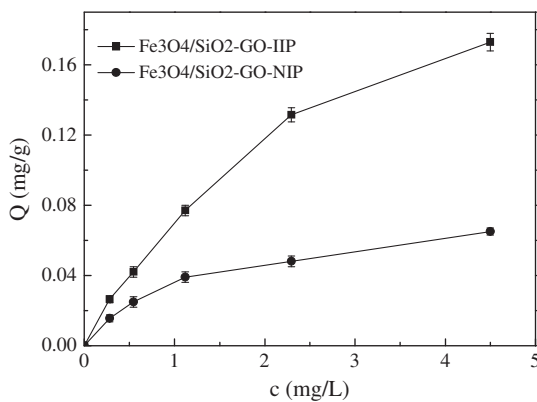


Fig. 9. Cr(III) ion adsorption isotherms for $\text{Fe}_3\text{O}_4/\text{SiO}_2\text{-GO-IIP}$ and $\text{Fe}_3\text{O}_4/\text{SiO}_2\text{-GO-NIP}$.

Table 2
Parameters obtained from different isotherm models

Models	Parameters		R^2
Langmuir	q_{max} (mg/g)	K_1 (L/mg)	0.9929
	0.25	0.42	
Freundlich	K_F (mg/g (mg/L) ⁿ)	n	0.9891
	0.07	1.43	

defined as the maximum capacity of adsorbent calculated from the Langmuir plots is 0.25 mg/g, which agreed closely with the calculation from Lagergren pseudo-second-order equation. The Freundlich parameters for n were higher than 1, indicating that Cr(III) was favorable for adsorption on adsorbents.

All the binding sites on the adsorbents were also assumed to be free sites that were prepared to accept

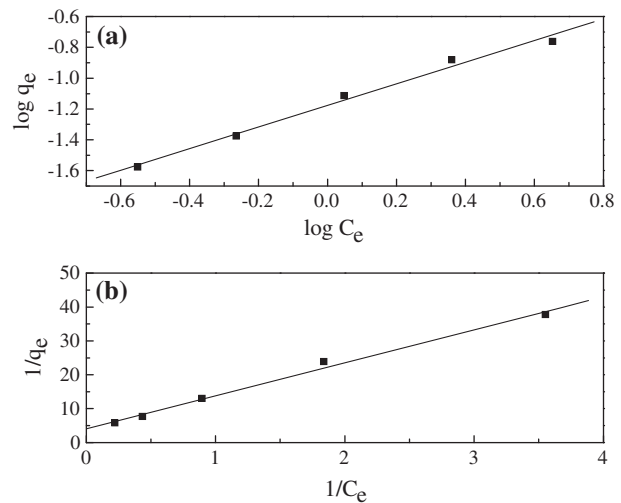


Fig. 10. Freundlich (a) and Langmuir (b) plot for the adsorption of Cr(III) on $\text{Fe}_3\text{O}_4/\text{SiO}_2\text{-GO-IIP}$.

Table 3
 R_L values in Langmuir isotherm of $\text{Fe}_3\text{O}_4/\text{SiO}_2\text{-GO-IIP}$

C_0 (mg/L)	R_L
0.25	0.904977
0.5	0.826446
1	0.704225
2	0.543478
4	0.373134

the adsorbents from the solution. The affinity between Cr(III) ion and Fe₃O₄/SiO₂-GO-IIP can be predicted using Langmuir dimensionless separation factor R_L given by the relation [30]

$$R_L = \frac{1}{1 + K_1 C_0} \quad (12)$$

where C_0 is the initial Cr(III) concentration (mg/L). R_L indicates the shape of the isotherm, and the values $R_L < 1$ and $R_L > 1$ represent favorable adsorption and unfavorable adsorption, respectively. The values of R_L are shown in Table 3. In this study, R_L values were all within 0 and 1, indicating a highly favorable adsorption with increasing adsorption efficiency at higher Cr(III) concentrations.

3.3. Adsorption selectivity

To evaluate the binding selectivity of Fe₃O₄/SiO₂-GO-IIP toward Cr(III), Na(I), Mg(II), and Ca(II) were selected as potential interferents due to their existence in wastewater containing chromium.

As seen in Fig. 11, the removal efficiencies for Cr(III), Na(I), Mg(II), and Ca(II) by Fe₃O₄/SiO₂-GO-IIP were 8.25, 3.46, 5.11, and 3.61%, respectively. These values show that Fe₃O₄/SiO₂-GO-IIP had the highest molecular recognition selectivity to Cr(III). The adsorption selectivity for Fe₃O₄/SiO₂-GO-NIP was low and its effects on the removal efficiency of Cr(III), Na(I), Mg(II), and Ca(II) were similar (3.14, 3.36, 3.92, and 3.68% respectively). The results indicated that Fe₃O₄/SiO₂-GO-NIP had no selectivity.

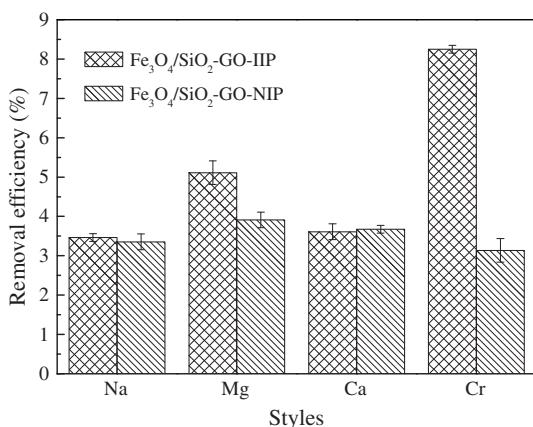


Fig. 11. The cross-reactivity of the Fe₃O₄/SiO₂-GO-IIP and Fe₃O₄/SiO₂-GO-NIP for adsorption of Cr(III) and interferents in aqueous medium.

The relative selectivity coefficient K' is an indicator that expresses an adsorption affinity of recognition sites to the imprinted Cr(III) ions. Table 4 summarizes the data of the distribution coefficients K_d , selectivity coefficients K , and relative selectivity coefficients K' of Na(I), Mg(II), and Ca(II) with respect to Cr(III).

The following information can be found in Table 1. (1) The selectivity coefficients of Fe₃O₄/SiO₂-GO-NIP for Cr(III) with respect to Na(I), Mg(II), and Ca(II) were lower, namely 0.933, 0.795, and 0.849, respectively; (2) The selectivity coefficients of Fe₃O₄/SiO₂-GO-IIP for Cr(III) with respect to Na(I), Mg(II), and Ca(II) were higher, namely 2.51, 1.67, and 2.40, respectively; and (3) The relative selectivity coefficients of Fe₃O₄/SiO₂-GO-IIP for Cr(III)/Na(I), Cr(III)/Mg(II), and Cr(III)/Ca(II) were 2.68, 2.10, and 2.83 times greater than Fe₃O₄/SiO₂-GO-NIP, respectively (Table 4).

The imprinted materials showed selectivity for the target molecule (i.e. Cr(III) ions) due to molecular geometry. This finding indicates that Cr(III) ions can be determined even in the presence of Na(I), Mg(II), and Ca(II) interferences because the cavities imprinted by Cr(III) were not matched to Na(I), Mg(II), and Ca(II) in size, shape, and spatial arrangement of combining sites. The ionic radii of Na(I) (102 pm), Mg(II) (72 pm), and Ca(II) (100 pm) were larger than those of Cr(III) (61.5 pm), so the entrance of Na(I), Mg(II), and Ca(II) into the cavity imprinted by Cr(III) was difficult. This phenomenon resulted in high recognition ability and high selectivity of Fe₃O₄/SiO₂-GO-IIP for Cr(III).

3.4. Desorption and reuse

Adsorbent regeneration is a potential key factor in improving wastewater process economics. Regenerations after exhaustion by sole Cr(III), Cr(III)/Na(I), Cr(III)/Na(I)/Mg(II), Cr(III)/Na(I)/Ca(II), and Cr(III)/Na(I)/Mg(II)/Ca(II) mixed solution were studied (Fig. 12). The desorption ratios of Cr(III) after the

Table 4
Adsorption selectivity of Fe₃O₄/SiO₂-GO-IIP and Fe₃O₄/SiO₂-GO-NIP

Metal ions	Fe ₃ O ₄ /SiO ₂ -GO-NIP		Fe ₃ O ₄ /SiO ₂ -GO-IIP		
	K_d (L/g)	K	K_d (L/g)	K	K'
Cr(III)	0.032	–	0.09	–	–
Na(I)	0.035	0.933	0.036	2.51	2.68
Mg(II)	0.041	0.795	0.054	1.67	2.10
Ca(II)	0.038	0.849	0.037	2.40	2.83

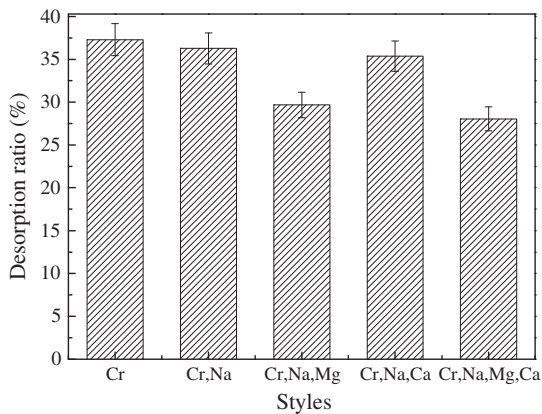


Fig. 12. Desorption of Cr(III) ions from $\text{Fe}_3\text{O}_4/\text{SiO}_2\text{-GO-IIP}$ by 0.1 M HCl.

desorption process reached equilibrium were about 37.29, 36.27, 29.68, 35.37, and 28.05%, respectively, indicating that the desorption ratio was not generally affected in a competing metal ion solution.

To test the stability and reusability of $\text{Fe}_3\text{O}_4/\text{SiO}_2\text{-GO-IIP}$, five binding/removal (regeneration) cycles were conducted using the same adsorbent in a batch experiment. No obvious decrease in the binding capacity was observed in pure Cr(III) solution (Fig. 13), which suggests good retention of the activity of $\text{Fe}_3\text{O}_4/\text{SiO}_2\text{-GO-IIP}$. The adsorption capacities of Cr(III) ions exhibited approximately 8% loss in Cr(III)/Na(I)/Mg(II)/Ca(II) mixed solution, which indicated that the adsorption capacity changed slightly when competing metal ions existed. This study also presented that the regeneration loss may be as much as 10%, even with well-operated systems [31]. In conclusion, $\text{Fe}_3\text{O}_4/\text{SiO}_2\text{-GO-IIP}$ can be used many times without decreasing its adsorption capacities significantly.

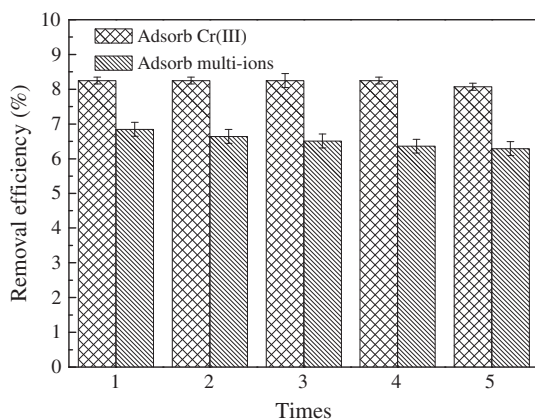


Fig. 13. Stability and potential regeneration of $\text{Fe}_3\text{O}_4/\text{SiO}_2\text{-GO-IIP}$ for removal of Cr(III).

4. Conclusions

Novel magnetic graphene oxide-based Cr(III) ion-imprinted materials were prepared by surface ionic imprinting technology, which can be efficiently used for adsorption of Cr(III) ions from aqueous solution. AEM, TEM, XRD, TGA, FTIR, and Raman spectroscopy were used to demonstrate the successful synthesis of $\text{Fe}_3\text{O}_4/\text{SiO}_2\text{-GO-IIP}$. The kinetic adsorption data agree with the intra-particle diffusion kinetic model. The kinetic experiment results indicated that the controlling step rate was mainly an intraparticle diffusion, although it was not the only rate-limiting step for Cr(III) ion adsorption. The equilibrium data fitted with the Langmuir adsorption isotherm equation. Langmuir dimensionless separation factor calculation results indicated that at higher Cr(III) ion concentrations, highly favorable adsorption with increased adsorption efficiency occurred. Competitive adsorption studies for Cr(III)/Na(I)/Mg(II)/Ca(II) mixed system showed that $\text{Fe}_3\text{O}_4/\text{SiO}_2\text{-GO-IIP}$ was highly selective to Cr(III) ions due to the imprinted cavity in the adsorbent. The relative selectivity coefficients of $\text{Fe}_3\text{O}_4/\text{SiO}_2\text{-GO-IIP}$ for Cr(III)/Na(I), Cr(III)/Mg(II), and Cr(III)/Ca(II) were 2.68, 2.10, and 2.83 times greater than those of $\text{Fe}_3\text{O}_4/\text{SiO}_2\text{-GO-NIP}$, respectively. The desorption ratio of $\text{Fe}_3\text{O}_4/\text{SiO}_2\text{-GO-IIP}$ was slightly affected by a competing metal ion solution. $\text{Fe}_3\text{O}_4/\text{SiO}_2\text{-GO-IIP}$ can be used five times without significantly decreasing its adsorption capacities. Therefore, $\text{Fe}_3\text{O}_4/\text{SiO}_2\text{-GO-IIP}$ can be considered a potential adsorbent in removing Cr(III) ions from aqueous solution due to its high affinity, selectivity, reusability, and easy separation.

Acknowledgments

This work was financially supported by Jilin Provincial Research Foundation for Basic Research, China (No. 20150520151JH), National Natural Science Foundation of China (No. 41401548) and Open Project of State Key Laboratory of Urban Water Resource and Environment, Harbin Institute of Technology (No. ES201510).

References

- [1] J. Romero-González, J.C. Walton, J.R. Peralta-Videa, E. Rodríguez, J. Romero, J.L. Gardea-Torresdey, Modeling the adsorption of Cr(III) from aqueous solution onto *Agave lechuguilla* biomass: Study of the advective and dispersive transport, *J. Hazard. Mater.* 161 (2009) 360–365.
- [2] C. Baggiani, G. Giraudi, C. Giovannoli, C. Tozzi, L. Anfossi, Adsorption isotherms of a molecular imprinted polymer prepared in the presence of a

- polymerisable template, *Anal. Chim. Acta* 504 (2004) 43–52.
- [3] T. Shiomi, M. Matsui, F. Mizukami, K. Sakaguchi, A method for the molecular imprinting of hemoglobin on silica surfaces using silanes, *Biomaterials* 26 (2005) 5564–5571.
- [4] C. Alvarez-Lorenzo, A. Concheiro, Molecularly imprinted polymers for drug delivery, *J. Chromatogr. B* 804 (2004) 231–245.
- [5] K. Araki, T. Maruyama, N. Kamiya, M. Goto, Metal ion-selective membrane prepared by surface molecular imprinting, *J. Chromatogr. B* 818 (2005) 141–145.
- [6] O. Brüggemann, Catalytically active polymers obtained by molecular imprinting and their application in chemical reaction engineering, *Biomol. Eng.* 18 (2001) 1–7.
- [7] O. Brüggemann, A. Visnjeviski, R. Burch, P. Patel, Selective extraction of antioxidants with molecularly imprinted polymers, *Anal. Chim. Acta* 504 (2004) 81–88.
- [8] R. Say, M. Erdem, A. Ersoz, H. Turk, A. Denizli, Biomimetic catalysis of an organophosphate by molecularly surface imprinted polymers, *Appl. Catal., A* 286 (2005) 221–225.
- [9] T.P. Rao, R. Kala, S. Daniel, Metal ion-imprinted polymers—Novel materials for selective recognition of inorganics, *Anal. Chim. Acta* 578 (2006) 105–116.
- [10] S. Haijia, Z. Ying, L. Jia, T. Tianwei, Biosorption of Ni^{2+} by the surface molecular imprinting adsorbent, *Process Biochem.* 41 (2006) 1422–1426.
- [11] J.H. Chen, G.P. Li, Q.L. Liu, J.C. Ni, W.B. Wu, J.M. Lin, Cr(III) ionic imprinted polyvinyl alcohol/sodium alginate (PVA/SA) porous composite membranes for selective adsorption of Cr(III) ions, *Chem. Eng. J.* 165 (2010) 465–473.
- [12] F. An, B. Gao, Adsorption characteristics of Cr(III) ionic imprinting polyamine on silica gel surface, *Desalination* 249 (2009) 1390–1396.
- [13] A.H. Lu, E.L. Salabas, F. Schüth, Magnetic nanoparticles: Synthesis, protection, functionalization, and application, *Angew. Chem. Int. Ed.* 46 (2007) 1222–1244.
- [14] T. Jing, H. Du, Q. Dai, H. Xia, J. Niu, Q. Hao, S. Mei, Y. Zhou, Magnetic molecularly imprinted nanoparticles for recognition of lysozyme, *Biosens. Bioelectron.* 26 (2010) 301–306.
- [15] X. Kan, Q. Zhao, D. Shao, Z. Geng, Z. Wang, J.-J. Zhu, Preparation and recognition properties of bovine hemoglobin magnetic molecularly imprinted polymers, *J. Phys. Chem. B* 114 (2010) 3999–4004.
- [16] Y. Ren, M. Zhang, D. Zhao, Synthesis and properties of magnetic Cu(II) ion imprinted composite adsorbent for selective removal of copper, *Desalination* 228 (2008) 135–149.
- [17] H. Li, Z. Chi, J.Z. Li, Covalent bonding synthesis of magnetic graphene oxide nanocomposites for Cr(III) removal, *Desalin. Water Treat.* 52 (2014) 1937–1946.
- [18] Y. Zhang, B.A. Chen, L.M. Zhang, J. Huang, F.H. Chen, Z.P. Yang, J.L. Yao, Z.J. Zhang, Controlled assembly of Fe_3O_4 magnetic nanoparticles on graphene oxide, *Nanoscale* 3 (2011) 1446–1450.
- [19] Y. Prasanna Kumar, P. King, V.S.R.K. Prasad, Adsorption of zinc from aqueous solution using marine green algae—*Ulva fasciata* sp., *Chem. Eng. J.* 129 (2007) 161–166.
- [20] A. Ersöz, R. Say, A. Denizli, Ni(II) ion-imprinted solid-phase extraction and preconcentration in aqueous solutions by packed-bed columns, *Anal. Chim. Acta* 502 (2004) 91–97.
- [21] C. Thomsen, S. Reich, Double resonant Raman scattering in graphite, *Phys. Rev. Lett.* 85 (2000) 5214–5217.
- [22] W.S. Choi, S.H. Choi, B. Hong, D.G. Lim, K.J. Yang, J.H. Lee, Effect of hydrogen plasma pretreatment on growth of carbon nanotubes by MPECVD, *Mater. Sci. Eng. C* 26 (2006) 1211–1214.
- [23] K.N. Kudin, B. Ozbas, H.C. Schniepp, Raman spectra of graphite oxide and functionalized graphene sheets, *Nano Lett.* 8 (2008) 36–41.
- [24] H.A. Becerril, J. Mao, Z. Liu, R.M. Stoltenberg, Z. Bao, Y. Chen, Evaluation of solution-processed reduced graphene oxide films as transparent conductors, *ACS Nano* 2 (2008) 463–470.
- [25] H.C. Schniepp, J.-L. Li, M.J. McAllister, H. Sai, M. Herrera-Alonso, D.H. Adamson, Functionalized single graphene sheets derived from splitting graphite oxide, *J. Phys. Chem. B* 110 (2006) 8535–8539.
- [26] S. Lagergren, About the theory of so-called adsorption of soluble substances, *Kungliga Svenska Vetenskapsakademiens Handlingar* 24 (1898) 1–39.
- [27] Y.S. Ho, G. McKay, D.A.J. Wase, C.F. Forster, Study of the sorption of divalent metal ions on to peat, *Adsorpt. Sci. Technol.* 18 (2000) 639–650.
- [28] R.S. Juang, M.L. Chen, Application of the Elovich equation to the kinetics of metal sorption with solvent-impregnated resins, *Indus. Eng. Chem. Res.* 36 (1997) 813–820.
- [29] S.K. Srivastava, R. Tyagi, N. Pant, Adsorption of heavy metal ions on carbonaceous material developed from the waste slurry generated in local fertilizer plants, *Water Res.* 23 (1989) 1161–1165.
- [30] B.H. Hameed, A.A. Rahman, Removal of phenol from aqueous solutions by adsorption onto activated carbon prepared from biomass material, *J. Hazard. Mater.* 160 (2008) 576–581.
- [31] S. Meenakshi, N. Viswanathan, Identification of selective ion-exchange resin for fluoride sorption, *J. Colloid Interface Sci.* 308 (2007) 438–450.